

QAOA with $N \cdot p \geq 200$

Ruslan Shaydulin and Marco Pistoia

Global Technology Applied Research, JPMorgan Chase, New York

Abstract

One of the central goals of the DARPA Optimization with Noisy Intermediate-Scale Quantum (ONISQ) program is to implement a hybrid quantum/classical optimization algorithm with high $N \cdot p$, where N is the number of qubits and p is the number of alternating applications of parameterized quantum operators in the protocol. In this note, we demonstrate the execution of the Quantum Approximate Optimization Algorithm (QAOA) applied to the MaxCut problem on non-planar 3-regular graphs with $N \cdot p$ of up to 300 on the Quantinuum H1-1 trapped-ion quantum processor. To the best of our knowledge, this is the highest $N \cdot p$ demonstrated on hardware to date. Our demonstration highlights the rapid progress of quantum hardware.

Introduction

The Quantum Approximate Optimization Algorithm (QAOA) [1, 2] is one of the leading candidate algorithms for demonstrating better-than-classical performance on near-term quantum computers. As a consequence, the task of implementing QAOA on hardware has attracted a lot of attention. For example, the central goal of Technical Area 1 of the DARPA ONISQ program is to implement a quantum optimizer with high $N \cdot p$ [3], with $N \cdot p > 100$ as the target for Phase 1, and $N \cdot p > 10,000$ for Phase 2. Here, N refers to the number of qubits used, while p is the number of alternating applications of QAOA operators (commonly referred to as QAOA layers). QAOA has also been proposed as a scalable application-centric benchmark for quantum hardware [4].

In this note, we report a successful execution of QAOA applied to the MaxCut problem on 3-regular graphs with $N = 20$ and $p \geq 10$ on the Quantinuum H1-1 trapped-ion quantum processor. We consider an execution with p layers successful if, for all $1 \leq p' \leq p$, the solution quality at p' is greater than at $p' - 1$. For all problem instances considered, we observe that the solution quality obtained by the algorithm increases monotonically with p up to 10. For some instances we observe monotonic improvements for p as large as 15. To the best of our knowledge, this is the largest (in terms of $N \cdot p$) QAOA demonstration on gate-model quantum computers to date. We make the executed circuits along with the raw data obtained from hardware publicly available at <https://doi.org/10.5281/zenodo.7689982>.

Results

Problem Definition We consider the MaxCut problem on 3-regular graphs. The goal of MaxCut is to partition the set of nodes V of a graph $G = (V, E)$ into two disjoint subsets such that the number of edges in E spanning both parts is maximized. For a sequence of spins $z \in \{-1, 1\}^{|V|}$, the MaxCut objective is given by $\mathcal{C}(z) = \frac{1}{2} \sum_{(i,j) \in E} (1 - z_i z_j)$. This objective is encoded on qubits by a diagonal Hamiltonian $C = \frac{1}{2} \sum_{(i,j) \in E} (1 - z_i z_j)$, where z_k is a Pauli z acting on qubit k .

The quantum state prepared by QAOA circuit with p layers is then given by

$$|\beta, \gamma\rangle = \prod_{l=1}^p e^{-i\beta_l \sum_{j=1}^{|V|} x_j} e^{-i\gamma_l C} |+\rangle^{\otimes |V|},$$

where $|+\rangle^{\otimes |V|}$ is a uniform superposition over computational basis states and x_j is a Pauli x acting on qubit j . The central figures of merit are the expected objective value (expected cut in the case of

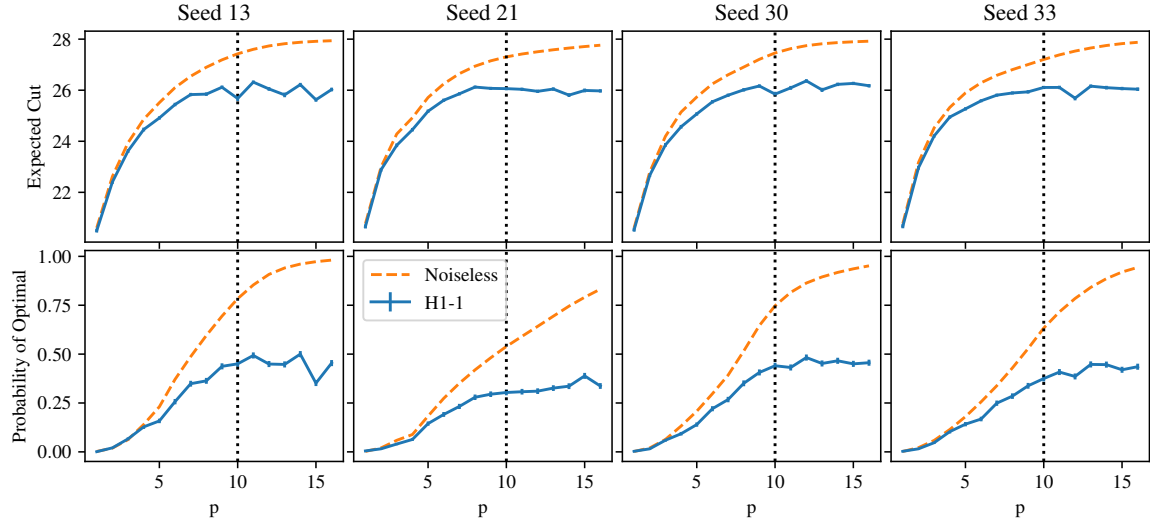


Figure 1: Values of the expected cut $\langle C \rangle$ (top), and probabilities p^{opt} of obtaining the optimal solution (bottom) for all instances executed. The optimal cut value for all graphs is 28 and the largest approximation ratio observed on hardware is 0.94. The probability of obtaining the optimal solution increases monotonically for all instances until $p = 10$ (black vertical dotted line). Error bars show one standard error of the mean.

MaxCut), given by

$$\langle C \rangle = \langle \beta, \gamma | C | \beta, \gamma \rangle = \sum_{z \in \{0,1\}^{|V|}} \Pr(z) \mathcal{C}(z),$$

and the probability of obtaining the optimal solution when measuring the QAOA state, denoted as p^{opt} . As can be easily seen, if the parameters are optimized with respect to a given metric, the correspondingly defined solution quality of QAOA can only increase with the number of layers p in the absence of noise. A noisy device introduces a trade-off between the improvements in solution quality and the increased probability of error from adding more layers. This means that, in practice, there is a depth beyond which adding more layers is not beneficial. In general, this depth is higher if the error rates are lower, motivating the use of $N \cdot p$ as an application-centric measure of device performance.

Experimental Setup The instances are created by generating random 3-regular graphs and post-selecting on the value of optimal cut being at least 28. We observe that the MaxCut problem for graphs with higher value of optimal cut is harder for QAOA, i.e., higher values of p are required to approach optimal values of $\langle C \rangle$ and p^{opt} . Consequently, harder instances enable the demonstration of higher $N \cdot p$. In Figure 1 and Table 1, each graph is identified by the random seed used to generate it.

We optimize parameters β, γ with respect to expected solution quality $\langle C(\beta, \gamma) \rangle$. For $p \leq 11$, we run one local optimization using COBYLA [5] initialized with fixed-angle parameters [6] obtained from QAOAKit [7]. For $p > 11$, we re-parameterize QAOA using the FOURIER scheme [8] with $q = p$ and run one local optimization using COBYLA [5] initialized with parameters extrapolated from $p' = p - 1$. The circuit with optimized parameters is compiled into the native gate set of the Quantinuum H1-1 device using the TKET transpiler [9], with each $z_i z_j$ term in the cost operator $e^{-i\gamma_i C}$ implemented using one ZZPhase native two-qubit gate. Therefore, the two-qubit gate count for each circuit is exactly $p \cdot |E| = 30p$. We remark that for the trapped-ion architecture of the H1-1 processor, the idling and crosstalk errors are low compared to the two-qubit gate errors. Combined with long coherence time, this leads to the success of the circuit execution being defined primarily by the two-qubit gate count, as opposed to the two-qubit gate depth. This is in contrast to superconducting architectures, for which the two-qubit gate depth is more predictive of performance than the two-qubit gate count due to the shorter coherence time and relatively higher crosstalk and idling errors.

p	$\langle C \rangle_{\text{H1-1}}$	$\langle C \rangle_{\text{ex}}$	$p_{\text{H1-1}}^{\text{opt}}$	$p_{\text{ex}}^{\text{opt}}$	p	$\langle C \rangle_{\text{H1-1}}$	$\langle C \rangle_{\text{ex}}$	$p_{\text{H1-1}}^{\text{opt}}$	$p_{\text{ex}}^{\text{opt}}$
1	20.500 ± 0.073	20.610	0.001 ± 0.001	0.002	1	20.663 ± 0.078	20.774	0.005 ± 0.002	0.002
2	22.405 ± 0.073	22.620	0.021 ± 0.004	0.019	2	22.886 ± 0.073	22.993	0.016 ± 0.004	0.020
3	23.620 ± 0.075	23.944	0.066 ± 0.008	0.063	3	23.843 ± 0.072	24.286	0.040 ± 0.006	0.059
4	24.460 ± 0.074	24.861	0.128 ± 0.010	0.140	4	24.453 ± 0.068	24.922	0.063 ± 0.008	0.089
5	24.913 ± 0.066	25.512	0.158 ± 0.011	0.231	5	25.177 ± 0.066	25.715	0.145 ± 0.011	0.183
6	25.439 ± 0.067	26.101	0.257 ± 0.014	0.371	6	25.606 ± 0.063	26.249	0.191 ± 0.012	0.274
7	25.829 ± 0.066	26.547	0.349 ± 0.015	0.487	7	25.858 ± 0.062	26.649	0.232 ± 0.013	0.351
8	25.846 ± 0.068	26.900	0.363 ± 0.015	0.595	8	26.123 ± 0.059	26.941	0.279 ± 0.014	0.419
9	26.116 ± 0.069	27.189	0.438 ± 0.016	0.694	9	26.071 ± 0.060	27.150	0.295 ± 0.014	0.481
10	25.675 ± 0.097	27.426	0.450 ± 0.016	0.784	10	26.062 ± 0.064	27.304	0.304 ± 0.014	0.539
11	26.316 ± 0.065	27.601	0.493 ± 0.016	0.854	11	26.035 ± 0.064	27.418	0.308 ± 0.014	0.591
12	26.050 ± 0.072	27.734	0.449 ± 0.016	0.908	12	25.956 ± 0.065	27.506	0.311 ± 0.014	0.642
13	25.816 ± 0.091	27.821	0.447 ± 0.016	0.941	13	26.045 ± 0.066	27.584	0.326 ± 0.015	0.694
14	26.219 ± 0.068	27.878	0.500 ± 0.016	0.961	14	25.808 ± 0.073	27.651	0.336 ± 0.015	0.745
15	25.625 ± 0.078	27.914	0.352 ± 0.015	0.973	15	25.990 ± 0.075	27.710	0.389 ± 0.015	0.791
16	26.026 ± 0.071	27.938	0.454 ± 0.016	0.981	16	25.973 ± 0.065	27.762	0.337 ± 0.015	0.832

(a) Seed 13

(b) Seed 21

p	$\langle C \rangle_{\text{H1-1}}$	$\langle C \rangle_{\text{ex}}$	$p_{\text{H1-1}}^{\text{opt}}$	$p_{\text{ex}}^{\text{opt}}$	p	$\langle C \rangle_{\text{H1-1}}$	$\langle C \rangle_{\text{ex}}$	$p_{\text{H1-1}}^{\text{opt}}$	$p_{\text{ex}}^{\text{opt}}$
1	20.537 ± 0.076	20.610	0.003 ± 0.002	0.002	1	20.673 ± 0.080	20.774	0.003 ± 0.002	0.002
2	22.671 ± 0.073	22.797	0.016 ± 0.004	0.020	2	22.963 ± 0.075	23.167	0.016 ± 0.004	0.021
3	23.857 ± 0.072	24.195	0.060 ± 0.007	0.064	3	24.208 ± 0.067	24.525	0.047 ± 0.007	0.059
4	24.568 ± 0.071	25.146	0.093 ± 0.009	0.132	4	24.948 ± 0.063	25.327	0.104 ± 0.010	0.114
5	25.070 ± 0.067	25.733	0.140 ± 0.011	0.208	5	25.269 ± 0.064	25.894	0.142 ± 0.011	0.180
6	25.547 ± 0.066	26.248	0.221 ± 0.013	0.297	6	25.585 ± 0.059	26.293	0.168 ± 0.012	0.256
7	25.803 ± 0.064	26.604	0.268 ± 0.014	0.392	7	25.806 ± 0.060	26.582	0.249 ± 0.014	0.338
8	26.015 ± 0.067	26.906	0.351 ± 0.015	0.516	8	25.892 ± 0.061	26.806	0.285 ± 0.014	0.429
9	26.165 ± 0.065	27.210	0.406 ± 0.015	0.646	9	25.936 ± 0.068	27.006	0.338 ± 0.015	0.528
10	25.847 ± 0.091	27.459	0.440 ± 0.016	0.747	10	26.107 ± 0.063	27.204	0.375 ± 0.015	0.633
11	26.092 ± 0.075	27.628	0.432 ± 0.015	0.816	11	26.108 ± 0.068	27.384	0.408 ± 0.015	0.716
12	26.365 ± 0.066	27.745	0.482 ± 0.016	0.864	12	25.688 ± 0.086	27.532	0.386 ± 0.015	0.784
13	26.013 ± 0.081	27.818	0.452 ± 0.016	0.895	13	26.158 ± 0.066	27.653	0.447 ± 0.016	0.841
14	26.229 ± 0.067	27.865	0.466 ± 0.016	0.918	14	26.100 ± 0.071	27.751	0.446 ± 0.016	0.886
15	26.266 ± 0.064	27.896	0.450 ± 0.016	0.936	15	26.064 ± 0.067	27.824	0.420 ± 0.015	0.920
16	26.175 ± 0.067	27.919	0.456 ± 0.016	0.952	16	26.039 ± 0.068	27.875	0.436 ± 0.015	0.944

(c) Seed 30

(d) Seed 33

Table 1: Expected values of cut ($\langle C \rangle$) and probabilities of obtaining the optimal solution (p^{opt}) with the corresponding standard error of the mean for all instances executed. $\langle C \rangle_{\text{ex}}$ and $p_{\text{ex}}^{\text{opt}}$ are obtained in exact noiseless simulation. Note that for most instances p^{opt} continues to improve beyond $p = 10$. The last p for which the p^{opt} is still increasing is highlighted in bold.

QAOA on the H1-1 Trapped-Ion Processor We present the results obtained on the Quantinuum H1-1 quantum processor in Figure 1. The complete results presented in Figure 1 are listed in Table 1 for completeness. The executed circuits and the raw data obtained from the device are available at <https://doi.org/10.5281/zenodo.7689982>. We use the probability p^{opt} of obtaining the optimal cut as the measure of solution quality for the purposes of defining a “successful execution”.

We observe that for all four graphs considered, the probability p^{opt} of obtaining the optimal cut grows monotonically up to $p = 10$, meaning that the experiments consistently succeed at $N \cdot p = 200$. This corresponds to 300 native two-qubit ZZPhase gates. We obtain approximation ratios of up to 0.94. To the best of our knowledge, this is the largest QAOA execution in terms of $N \cdot p$ to date. We refer the interested reader to Table 2 in Ref. [10] for an overview of previous state-of-the-art demonstrations. We remark that alternative definitions of QAOA layer may lead to smaller circuits that have higher $N \cdot p$. For example, in the recently introduced mixer-phaser ansatz [11], each “layer” can be implemented using only 3 CNOTs. If “layer” is to be redefined in this way, our results indicate that $N \cdot p \geq 2000$ would become within reach for current hardware. However, in this note we focus on the original QAOA definition.

We note that p^{opt} continues to grow for higher p compared to the expected solution quality $\langle C \rangle$, which for some instances stops increasing at $p = 9$. We conjecture that this difference is due to higher p required to saturate the success probability in the noiseless case. This conjecture is supported by the observation that the highest $N \cdot p$ is achieved with instances for which $p_{\text{ex}}^{\text{opt}}$ grows the slowest. For example, the instance labelled “Seed 21” achieves $N \cdot p = 300$ and $p_{\text{ex}}^{\text{opt}} = 0.791$ at $p = 15$. In contrast, the same $p_{\text{ex}}^{\text{opt}}$ is reached at $p = 11$ for “Seed 13” and “Seed 30”, and $N \cdot p$ is correspondingly lower. We further note that neither $\langle C \rangle$ nor p^{opt} measurably decrease as more layers are added. This is in contrast to previous results on superconducting quantum processors [12, 13], where at some point

additional layers begin to introduce an amount of noise sufficient to significantly decrease the expected solution quality. Combined, these observations suggest that the current experiment is not yet limited by the gate fidelity of the device. Higher values of $N \cdot p$ may be achieved at current gate fidelities either by considering harder problems (higher p) or by loading more ions into the trap (higher N).

Acknowledgements

The authors thank Dylan Herman, Changhao Li, Yue Sun and other members of the Global Technology Applied Research center of JPMorgan Chase for helpful discussions and providing feedback on the manuscript.

References

- [1] Tad Hogg and Dmitriy Portnov. Quantum optimization. *Information Sciences*, 128(3-4):181–197, 2000. [doi:10.1016/s0020-0255\(00\)00052-9](https://doi.org/10.1016/s0020-0255(00)00052-9).
- [2] Edward Farhi, Jeffrey Goldstone, and Sam Gutmann. A quantum approximate optimization algorithm. *arXiv:1411.4028*, 2014. [doi:10.48550/arXiv.1411.4028](https://doi.org/10.48550/arXiv.1411.4028).
- [3] DARPA Broad Agency Announcement: Optimization with noisy intermediate-scale quantum devices (ONISQ), Apr 2019. URL: <https://www.grants.gov/web/grants/view-opportunity.html?oppId=314702>.
- [4] Simon Martiel, Thomas Ayral, and Cyril Allouche. Benchmarking quantum coprocessors in an application-centric, hardware-agnostic, and scalable way. *IEEE Transactions on Quantum Engineering*, 2:1–11, 2021. [doi:10.1109/tqe.2021.3090207](https://doi.org/10.1109/tqe.2021.3090207).
- [5] M. J. D. Powell. A direct search optimization method that models the objective and constraint functions by linear interpolation. In *Advances in Optimization and Numerical Analysis*, pages 51–67. Springer Netherlands, 1994. [doi:10.1007/978-94-015-8330-5_4](https://doi.org/10.1007/978-94-015-8330-5_4).
- [6] Jonathan Wurtz and Danylo Lykov. Fixed-angle conjectures for the quantum approximate optimization algorithm on regular MaxCut graphs. *Physical Review A*, 104(5), Nov 2021. [doi:10.1103/physreva.104.052419](https://doi.org/10.1103/physreva.104.052419).
- [7] Ruslan Shaydulin, Kunal Marwaha, Jonathan Wurtz, and Phillip C Lotshaw. QAOAKit: A toolkit for reproducible study, application, and verification of QAOA. In *Second International Workshop on Quantum Computing Software*, 2021. [doi:10.1109/QCS54837.2021.00011](https://doi.org/10.1109/QCS54837.2021.00011).
- [8] Leo Zhou, Sheng-Tao Wang, Soonwon Choi, Hannes Pichler, and Mikhail D. Lukin. Quantum approximate optimization algorithm: Performance, mechanism, and implementation on near-term devices. *Physical Review X*, 10:021067, 2020. [doi:10.1103/PhysRevX.10.021067](https://doi.org/10.1103/PhysRevX.10.021067).
- [9] Seyon Sivarajah, Silas Dilkes, Alexander Cowtan, Will Simmons, Alec Edgington, and Ross Duncan. $t|ket\rangle$: a retargetable compiler for NISQ devices. *Quantum Science and Technology*, 6(1):014003, Nov 2020. [doi:10.1088/2058-9565/ab8e92](https://doi.org/10.1088/2058-9565/ab8e92).
- [10] Pradeep Niroula, Ruslan Shaydulin, Romina Yalovetzky, Pierre Minssen, Dylan Herman, Shao-han Hu, and Marco Pistoia. Constrained quantum optimization for extractive summarization on a trapped-ion quantum computer. *Scientific Reports*, 12(1), Oct 2022. [doi:10.1038/s41598-022-20853-w](https://doi.org/10.1038/s41598-022-20853-w).
- [11] Ryan LaRose, Eleanor Rieffel, and Davide Venturelli. Mixer-phaser ansätze for quantum optimization with hard constraints. *Quantum Machine Intelligence*, 4(2), Jun 2022. [doi:10.1007/s42484-022-00069-x](https://doi.org/10.1007/s42484-022-00069-x).
- [12] Matthew P Harrigan, Kevin J Sung, Matthew Neeley, Kevin J Satzinger, Frank Arute, Kunal Arya, Juan Atalaya, Joseph C Bardin, Rami Barends, Sergio Boixo, et al. Quantum approximate optimization of non-planar graph problems on a planar superconducting processor. *Nature Physics*, 17(3):332–336, 2021. URL: <https://doi.org/10.1038/s41567-020-01105-y>.

[13] Nathan Lacroix, Christoph Hellings, Christian Kraglund Andersen, Agustin Di Paolo, Ants Remm, Stefania Lazar, Sebastian Krinner, Graham J. Norris, Mihai Gabureac, Johannes Heinsoo, Alexandre Blais, Christopher Eichler, and Andreas Wallraff. Improving the performance of deep quantum optimization algorithms with continuous gate sets. *PRX Quantum*, 1:110304, Oct 2020. [doi:10.1103/PRXQuantum.1.020304](https://doi.org/10.1103/PRXQuantum.1.020304).

Disclaimer

This paper was prepared for informational purposes by the Global Technology Applied Research center of JPMorgan Chase & Co. This paper is not a product of the Research Department of JPMorgan Chase & Co. or its affiliates. Neither JPMorgan Chase & Co. nor any of its affiliates makes any explicit or implied representation or warranty and none of them accept any liability in connection with this paper, including, without limitation, with respect to the completeness, accuracy, or reliability of the information contained herein and the potential legal, compliance, tax, or accounting effects thereof. This document is not intended as investment research or investment advice, or as a recommendation, offer, or solicitation for the purchase or sale of any security, financial instrument, financial product or service, or to be used in any way for evaluating the merits of participating in any transaction.